

The exoplanetary magnetosphere extension in Sun-like stars based on the solar wind - solar UV relation

Raffaele Reda,¹ Luca Giovannelli,^{1*} Tommaso Alberti,² Francesco Berrilli,¹ Luca Bertello,³
Dario Del Moro,¹ Maria Pia Di Mauro,² Piermarco Giobbi,¹ and Valentina Penza¹

¹*Department of Physics, University of Rome Tor Vergata, Via della Ricerca Scientifica 1, Rome, 00133, Italy*

²*INAF - Istituto di Astrofisica e Planetologia Spaziali, Via del Fosso del Cavaliere 100, Rome, 00133, Italy*

³*National Solar Observatory, 3665 Discovery Drive, 3rd Floor, Boulder, CO 80303, USA*

Accepted XXX. Received YYY; in original form ZZZ

ABSTRACT

Earth’s magnetosphere extension is controlled by solar activity level via solar wind properties. Understanding such a relation in the Solar System is useful to predict the condition of exoplanetary magnetosphere near Sun-like stars. We use measurements of a chromospheric proxy, the Ca II K index, and solar wind OMNI parameters to connect the solar activity variations on the decennial time scales to solar wind properties. The dataset span over the time interval 1965-2021, which almost entirely covers the last 5 solar cycles. Using both cross-correlation and mutual information analysis, a 3.2-year lag of the solar wind speed with respect to the Ca II K index is found. Analogously, a 3.6-year lag is found with respect to the dynamic pressure. A correlation between the solar wind dynamic pressure and the solar UV emission is therefore found and used to derive the Earth’s magnetopause standoff distance. Moreover, the advantage of using a chromospheric proxy, such as the Ca II K index, opens the possibility to extend the relation found for the Sun to Sun-like stars, by linking stellar variability to stellar wind properties. The model is applied to a sample of Sun-like stars as a case study, where we assume the presence of an Earth-like exoplanet at 1 AU. Finally, we compare our results with previous estimates of the magnetosphere extension for the same set of sun-like stars.

Key words: solar-terrestrial relations – solar wind – Sun: UV radiation – Stars: activity – Stars: solar-type – planet–star interactions

1 INTRODUCTION

The solar wind is a continuous plasma flow emitted from the upper atmosphere of the Sun, mostly consisting of ions and electrons (e.g. [Verscharen et al. 2019](#)). At 1 AU it is characterized by a typical speed ranging between 250 km/s and 800 km/s, a density of a few particles per cubic centimeter, and carries out a magnetic field of the order of a few nanoTeslas ([Parks 2018](#)) with a dependency over the solar activity cycle ([Poletto 2013](#)). During the last 40 years it has been investigated with increasing deeper details, both in terms of instrument resolution and spacecraft locations, allowing us to have a wide overview of its dynamical properties ([Escoubet et al. 1997](#); [Stone et al. 1998](#); [Burch et al. 2016](#)) also in connection with its origins which lie in the lower solar atmosphere where the Coronal Holes are the source of the fast solar wind (e.g. [Bryans et al. 2020](#)). It is considered as a natural laboratory to investigate several kind of processes and mechanisms as turbulence and intermittency, plasma instabilities, waves and structures, small- vs. large-scale dynamics, and so on (e.g. [Bavassano et al. 1998](#); [Bruno & Carbone 2016](#)). We can describe the solar wind as a multiscale system whose dynamics occurs over a wide range of scales. Looking at scales larger than the so-called inertial range (i.e., larger than a few hours) the dynamics of the solar wind is mainly related with solar source mechanisms as ac-

tive regions, coronal mass ejections, and flares ([Tu & Marsch 1995](#)). These large-scale phenomena are the main responsible for changing planetary environments when interacting with planetary magnetospheres and/or ionospheres, giving rise to a wide variety of processes as geomagnetic storms and substorms, particle precipitation, auroral activity, localized energy transfer processes, also in connection with the possible climate of extrasolar planets (e.g. [Russell 1993](#); [Blanc et al. 2005](#); [Airapetian et al. 2020](#); [Galuzzo et al. 2021](#)). A clear manifestation of the solar wind-magnetosphere interactions is the observed change of the standoff distance of the nose of the magnetospheric cavity, thus affecting both its size and shape. The standoff distance is indeed defined as the distance at which the solar wind dynamic pressure equals the magnetic pressure of the magnetospheric cavity, i.e.,

$$|\rho (\mathbf{v} \cdot \nabla) \mathbf{v}| \simeq \left| -\nabla \left(\frac{B^2}{8\pi} \right) \right|. \quad (1)$$

Assuming the incompressibility condition for the solar wind, i.e., a constant mass density $\rho = \rho_0$, and writing the magnetic field as a dipolar shape, i.e., $B = \frac{M_0}{r^3}$, being M_0 the Earth’s dipole moment, we can obtain the standoff distance as

$$R_s = \left(\frac{1}{4\pi\rho_0} \right)^{1/6} \left(\frac{M_0^2}{v^2} \right)^{1/6}. \quad (2)$$

* E-mail: luca.giovannelli@roma2.infn.it (LG)

Eq. 2 clearly relates the standoff distance R_s to the solar wind speed v (or the dynamic pressure) suggesting that it decreases as v increases. This means that the shape and the size of the Earth's magnetospheric cavity reduces as the solar wind dynamic pressure increases. In the last two decades several efforts have been made to increase our capabilities in forecasting the dynamical behaviour of the solar wind as well as its effects on Earth (Bothmer & Daglis 2007). Thus, investigating and characterising the relations between long-term solar activity proxies and in-situ solar wind measurements are of crucial impact for any Space Weather and Space Climate forecasting scheme and could be fundamental for characterizing Sun-like stars and their interaction with own planetary systems (e.g. Airapetian et al. 2020). Solar magnetic activity main periodicity is the well-known 11 years solar cycle. Periods close to 11 years have been found in most solar wind parameters since the very first observations from satellites (Siscoe et al. 1978; King 1979; Neugebauer 1981). However, a non perfect match of the solar wind long-term behaviour with the shape and phase of the sunspot cycle (Hirshberg 1973; Intriligator 1974; Feynman 1982) stimulated a discussion with the observed lag with geomagnetic indices. As longer time-series of near-Earth solar wind measurements became available, several studies investigated the periods of solar wind parameters and the relation between the Sunspot Number and solar wind proxies (Petrinec et al. 1991; Köhnlein 1996; El-Borie 2002; Katsavrias et al. 2012; Richardson & Cane 2012; Li et al. 2016, 2017; Venzmer & Bothmer 2018; Samsonov et al. 2019), or geomagnetic data such as the aa index (Echer et al. 2004; Dmitriev et al. 2005; Lockwood et al. 2009). However, this is the first study, to our knowledge, to analyse the near-Earth solar wind measurements in relation to Ca II K index over the last five solar cycles.

Starting from the 1960s astronomers started looking with particular attention to other "suns" (i.e., stars with physical properties quite similar to solar ones or Sun-like stars), with the aim to search for stellar cycles in solar analogs and to understand where the Sun stands on a broader context (Wilson 1968). To carry out this purpose, a long-term observational campaign regarding their emissions in Ca II H & K lines, expressed in terms of the dimensionless S-index (Wilson 1978; Vaughan et al. 1978), was conducted at Mount Wilson Observatory starting from 1966 (Wilson 1968) and then continued at Lowell Observatory starting from 1995 (see e.g., Hall & Lockwood 1998). The data provided by those surveys have enormously improved our knowledge about the long-term chromospheric variations of Sun-like stars as well as how these variations are connected with changes in brightness (see e.g., Skumanich 1972; Baliunas et al. 1995; Radick et al. 1998). When we study such type of stars the Sun represents a sort of Rosetta stone, so that our understanding about how its magnetic activity affects the solar-system planets can be seen as a starting point to assess the way Sun-like stars influence the environment around them. The goal of this work is to extend the model for the Earth's magnetosphere standoff distance based on the Ca II K index to exoplanets orbiting Sun-like stars. To accomplish this goal we take advantage of chromospheric measurements provided by both the above mentioned campaigns, selecting Sun-like stars that are in a faculae-dominated activity regime, as it is the Sun. Thus, we compute the exoplanet magnetospheric extension without the need of X-ray observations of the stellar corona, by linking the stellar magnetic variability with stellar wind properties.

2 DATASETS DESCRIPTION

To study the relation between solar magnetic variability and near-Earth solar wind parameters, we need to use datasets which cover a sufficiently extended time interval. As previously described, the magnetic activity of the Sun can be quantified by using different solar indices. For this work we use a physical index which measures the mean properties of the solar chromospheric emission: the Ca II K index. Monthly measurements of this index starting from 1907 and covering more than one century are public available from the National Solar Observatory (NSO)¹. The Ca II K index dataset contains measurements up to October 2017 but it is possible to use other solar activity proxies linked to chromospheric emission, such as the Mg II index (Vioreck et al. 2001), to extend the analysis almost to date.

Regarding the solar wind we use data available from OMNI database, which provides to date various near-Earth solar wind parameters at different time resolutions. In particular, we focus our attention on the hourly-resolution measurements of the plasma ion density n and speed v , from which we computed the solar wind dynamic pressure P , defined as $1/2 m_p n v^2$, where we assume proton mass (m_p) as the mean ion mass. The OMNI database provides plasma measurements only starting from 1965 and, therefore, covers a shorter time interval with respect to Ca II K index. This places a limit on the length of the time period over which a relation between solar proxies and solar wind parameters can be studied. Despite this, by using the Mg II index to reconstruct Ca II K index to date, the latter and the solar wind parameters time series have an overlapping time period which goes from July 1965 up to April 2021, covering almost entirely the last five solar cycles (SCs 20-24).

Starting from the monthly values of Ca II K index, solar wind speed and dynamic pressure, we follow the approach used by Köhnlein (1996) and apply a 37-month moving average to look at the long-term behaviour of these quantities. These time series are shown in Figure 1. The size of the time window used for the moving average allows to remove the effects of the solar variability related to the solar rotation and the yearly time-scales.

The availability of the observations in the Ca II H & K lines provided by the HK Project at the Mount Wilson Observatory (Wilson 1968, 1978; Duncan et al. 1991; Baliunas et al. 1995) is fundamental to extend the model calibrated on the Sun-Earth system to Sun-like stars systems. These measurements, which are accessible for thousand stars, constitute a broad and long dataset spanning nearly 30 years in many cases. We take advantage of the availability of such measurements to relate, in stars other than the Sun, the mean chromospheric emission to stellar wind dynamic pressure, and hence to study its impact on the exo-planetary magnetospheres.

In the following subsections a detailed description of the datasets used for this work will be provided.

2.1 Solar wind OMNI dataset

We used solar wind data coming from the OMNI dataset at 1-hour resolution freely retrieved at <https://cdaweb.gsfc.nasa.gov/cgi-bin/eval1.cgi>.

This dataset consists of a collection of solar wind magnetic field and plasma parameters data coming from several spacecraft located near the L1 Lagrangian point at a distance of ~ 200 Earth radii. The measurements taken at L1 are then shifted to the nose of the

¹ <https://solis.nso.edu/0/iss/>

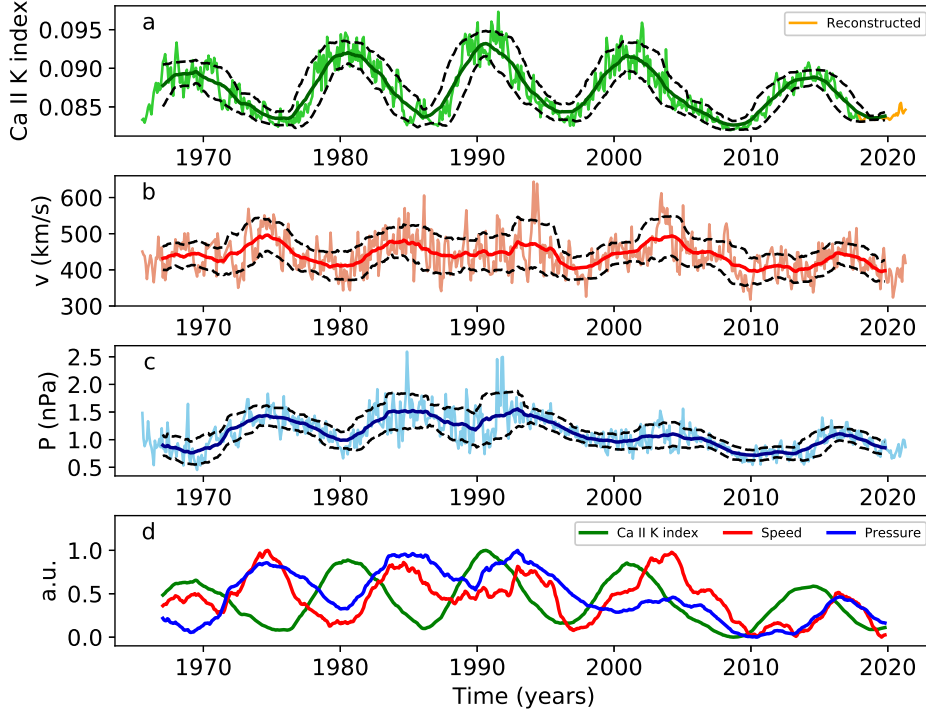


Figure 1. Monthly means (light colours) and superimposed 37-month moving averages (dark colours) of: a) Ca II K index, b) Solar Wind speed and c) Solar Wind dynamic pressure. In the upper panel, the orange line shows the reconstructed Ca II K index obtained using Mg II index. d) Comparison of Ca II K index (green), SW speed (red) and SW dynamic pressure (blue) normalized between 0 and 1. In panels a, b and c the dashed lines indicate the 1-sigma confidence interval.

bow shock (~ 14 Earth radii) by considering several factors as the geometry of the Earth-spacecraft separation vector, the shape and the orientation of the solar wind variation phase front and the direction of the solar wind flow (Weimer et al. 2002, 2003). By assuming that solar wind parameters’ values lie on a planar surface (i.e., the phase front) convected by the solar wind we are able to propagate what is observed at the L1 point to a different place at the time that the phase front sweeps over that location (Weimer & King 2008). The family of spacecraft considered for building up the OMNI database is formed by IMP, ISEE, ACE, Wind, and Geotail (King & Papitashvili 2005), thus allowing to cover the period from 1965 to date (Richardson & Paularena 2001).

2.2 Ca II index and Mg II index datasets

The Ca II K 0.1 nm emission index data are derived from the series of spectroheliograms taken at Kodaikanal Solar Observatory (India, 1907 - 2013), the K-line monitor program of disk-integrated measurements from the National Solar Observatory (NSO) at Sacramento Peak (USA, 1976 - 2015), and from the Integrated Sunlight Spectrometer on the Synoptic Optical Long-term Investigations of the Sun (SOLIS) telescope managed by NSO (USA, 2006 - 2017). Since October 2017 the SOLIS facility is offline, pending its relocation to a permanent site at Big Bear Solar Observatory (California, USA). The procedure to combine these three data sets into a single disk-integrated Ca II K 0.1 nm emission index time series composite is described in Bertello et al. (2016).

As previously seen, monthly values of the Ca II K index are not available later than October 2017. This lack of data can be over-

come by using other physical indices related to the chromospheric emission of the Sun, whose measurements are available to date. To this scope, we use the Mg II composite from the University of Bremen, which is derived from combining several satellite instruments (Viereck et al. 2004) and has been proven to be an excellent proxy for the solar UV irradiance (Dudok de Wit et al. 2009) in particular related to the interaction with the circumterrestrial environment (Bigazzi et al. 2020). The Mg II index, defined as the core-to-wing ratio of the Mg II doublet centered at 280 nm, is freely accessible with daily resolution since November 1978². Starting from the daily values, we calculate the monthly means of Mg II index and we note that, in the time interval November 1978 - October 2017, the latter strongly correlate with Ca II K index ($r = 0.95$). Then, by using the linear relation $\text{Ca II K} = 0.5619 \text{ Mg II} - 0.0014$, we extend the monthly dataset of Ca II K index until April 2021.

2.3 Mount Wilson Observatory dataset

The first long term observational campaign to study and characterize the magnetic activity behaviour of stars other than the Sun, named HK Project, has been conducted at the Mount Wilson Observatory. To search for stellar analogues to the solar cycle, the emission in the chromospheric H (393.4 nm) and K (396.8 nm) lines of the Ca II has been monitored from 1966 to 1995 for thousands stars (Wilson 1968, 1978; Duncan et al. 1991; Baliunas et al. 1995). The measurements from the MWO are expressed in term of the S-index, a dimensionless quantity which is defined as the ratio of emission in the Ca II

² <http://www.iup.uni-bremen.de/UVSAT/Datasets/mgii>

H & K line cores to that in two nearby reference bandpasses (see the definition provided by [Vaughan et al. \(1978\)](#) for further details). These observations enabled to place the Sun in a more wide stellar context and have constituted, during the last decades, an important basis for studying processes analogs to solar activity and cycle, as well as how they are related to stellar properties ([Vaughan & Preston 1980](#); [Durney et al. 1981](#); [Baliunas et al. 1995](#); [Saar & Brandenburg 1999](#); [Hall 2008](#); [Oláh et al. 2016](#)). Moreover, they have allowed to study the way chromospheric variability is connected with changes in brightness, whose phase difference reveals the stellar dynamo activity regime, spot-dominated (anti-phase) or faculae-dominated (phase) ([Radick et al. 1998](#); [Reinhold et al. 2019](#)). Recently, the Mount Wilson HK Project data for almost 2300 stars have been released by the National Solar Observatory (NSO)³.

3 LONG-TERM CORRELATIONS OF SOLAR WIND PARAMETERS AND SOLAR ACTIVITY

As a first step for this analysis we assess the relationship between solar activity and solar wind parameters by computing the Pearson's correlation coefficient over the whole time extent of the dataset. As depicted in the scatter plots of Figure 2, we found an almost zero correlation coefficient ($r = -0.01$) between Ca II K index and solar wind speed, with a similar result also for the dynamic pressure ($r = 0.01$). Hence, in the whole time interval which goes from July 1965 to April 2021, we do not found a significant correlation (the p-value is higher than 0.05) between Ca II K index and the solar wind parameters. As shown in previous studies, the declining phase of solar cycles are characterized by the presence of high speed solar wind streams ([Gosling et al. 1976](#); [Luhmann et al. 2009](#); [Tokumaru et al. 2010](#); [Richardson & Cane 2012](#)), which significantly affect the long-term averages of the solar wind speed. Thus, it is reasonable to expect that solar activity and solar wind response can be related taking into account a time lag. To investigate this hypothesis we compute the cross-correlation between Ca II K index and solar wind speed, where we assume that the latter has a delayed response to changes in solar activity, which means that we are considering only positive time lags of the solar wind with respect to Ca II K index (the result for negative lags is also shown for completeness). As shown in the top panel of Figure 3, the correlation coefficient between the two quantities peaks, with a value of 0.65, at time lag of 3.2 ± 0.1 years. The two time-series as visible in the panel b of Figure 3, where the solar wind speed has been back-shifted by the time lag found, have a quite similar phase when a time delay is considered. This result is quite in agreement to that reported by [Li et al. \(2016\)](#), which found that the daily means of the solar wind velocity lag the ones of SSN by about 3 years (see their fig. 3). A 3-year time shift was also brought out by [Venzmer & Bothmer \(2018\)](#) for the correlation of the yearly averages of the same quantities.

A slightly bigger time lag has been found performing the cross-correlation of Ca II K index with solar wind dynamic pressure. In this case, we obtain a correlation coefficient of 0.57 for a time lag of 3.6 ± 0.1 years, as shown in the panel c of Figure 3.

By taking into account the above time lags, as obtained from cross-correlation analysis, we found linear relations for the Ca II K index with both solar wind speed and dynamic pressure. The relationship between these quantities is shown in the two scatter plot in Figure 4, where the two black lines show the best linear fits to the

data points. The corresponding empirical equations are the following ones:

$$v \text{ (km/s)} = (5930 \pm 280) \text{ Ca II K} - (76 \pm 24). \quad (3)$$

$$P \text{ (nPa)} = (49.1 \pm 2.8) \text{ Ca II K} - (3.17 \pm 0.24); \quad (4)$$

We can conclude that, by considering the time delay, the correlation coefficients between Ca II K index and the two solar wind parameters investigated significantly increase. Similar results were recently reported by [Samsonov et al. \(2019\)](#). By using yearly averaged data for the last five solar cycles, they found the maximum correlation of both solar wind speed and dynamic pressure with SSN taking into account a 3-year time lag. In particular, they found a correlation coefficient $r = 0.57$ between SSN and SW dynamic pressure for 3-year time lag, in line with our results of $r = 0.57$ for 3.6-year lag. Moreover, they found $r = 0.68$ focusing only over the last three solar cycles taking 2-year lag, which is exactly the value we found for 2.4-year lag over the same cycles.

To assess our results in a stronger framework we also explored the nonlinear features of shared information between the Ca II K index and solar wind parameters. To do this, we used the mutual information analysis ([Shannon 1948](#)). Given a pair of time series $(x(t_j), y(t_k))$ the mutual information coefficient (MI) is defined as

$$MI = \sum_{j,k} p(x(t_j), y(t_k)) \log \frac{p(x(t_j), y(t_k))}{p(x(t_j))p(y(t_k))} \quad (5)$$

where $p(x, y)$ is the joint probability of observing the pair of values (x, y) , while $p(x)$ and $p(y)$ are the independent distributions. For statistically independent time series $MI = 0$, while for correlated time series $MI \geq MI_{th}$, a threshold associated with a particular statistical significance level (e.g., 95%, as in this case).

As reported in Figure 5 the mutual information reaches its maximum for time delays ~ 3.2 yr and ~ 3.4 yr which are consistent with those estimated via the cross-correlation analysis (see Figure 3). This seems to suggest that a linear relation exists between the Ca II K index and solar wind parameters, thus in the following we use the results from cross-correlation analysis.

4 MAGNETOSPHERE EXTENSION

In the previous section, we found a relation which allows to connect the 37-month moving averages of a solar UV proxy, the Ca II K index, to the solar wind dynamic pressure. Once the latter is known, the size of the Earth's magnetosphere on the day-side can be calculated by balancing the planetary magnetic pressure with the solar wind dynamic ram pressure. Starting from the relation by [Griebmeier et al. \(2004\)](#), we introduce the following equation:

$$R_{MP} = \left[\frac{\mu_0 f_0^2 M_E^2}{8\pi^2 10^{-9} (\alpha \text{ Ca II K} + \beta)} \right]^{1/6} \quad (6)$$

where $\alpha = 49.14$ and $\beta = -3.17$ are the parameters of the linear regression from the previous section, μ_0 is the vacuum permeability, M_E is the Earth's magnetic moment, while f_0 is a form factor to take into account for the non-spherical shape of the Earth's magnetosphere. For the latter two parameters we assume the same values as in [See et al. \(2014\)](#), which are respectively $M_E = 8 \cdot 10^{22} \text{ Am}^2$ and $f_0 = 1.16$. Figure 6 shows the Earth's magnetopause standoff distance computed by using Eq. 6 for two cases: 37-month moving average series by taking into account for the 3.6-year lag

³ <https://nso.edu/data/historical-data/mount-wilson-observatory/hk-project/>

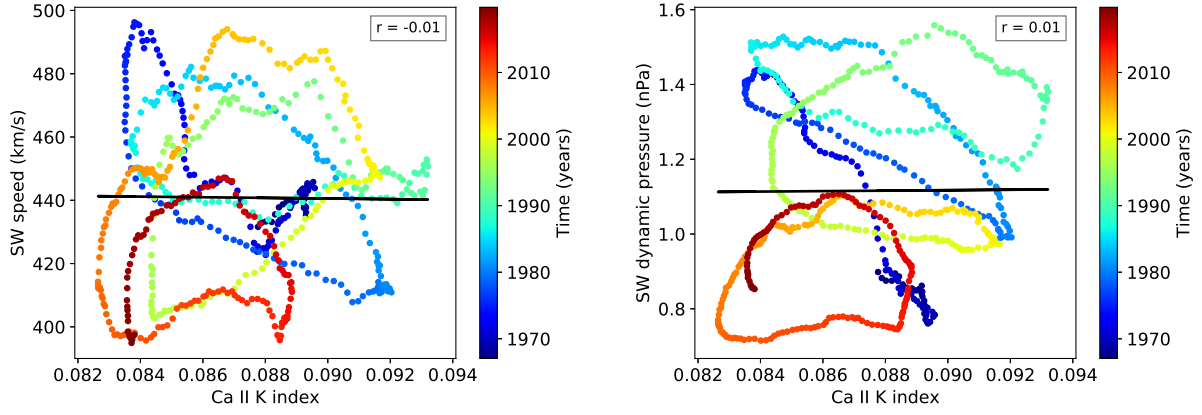


Figure 2. Scatter plot of 37-month moving averages of Ca II K index and, respectively, solar wind speed (left panel) and solar wind dynamic pressure (right panel). The time is represented by the color map. The correlation coefficient is, respectively, -0.01 and 0.01.

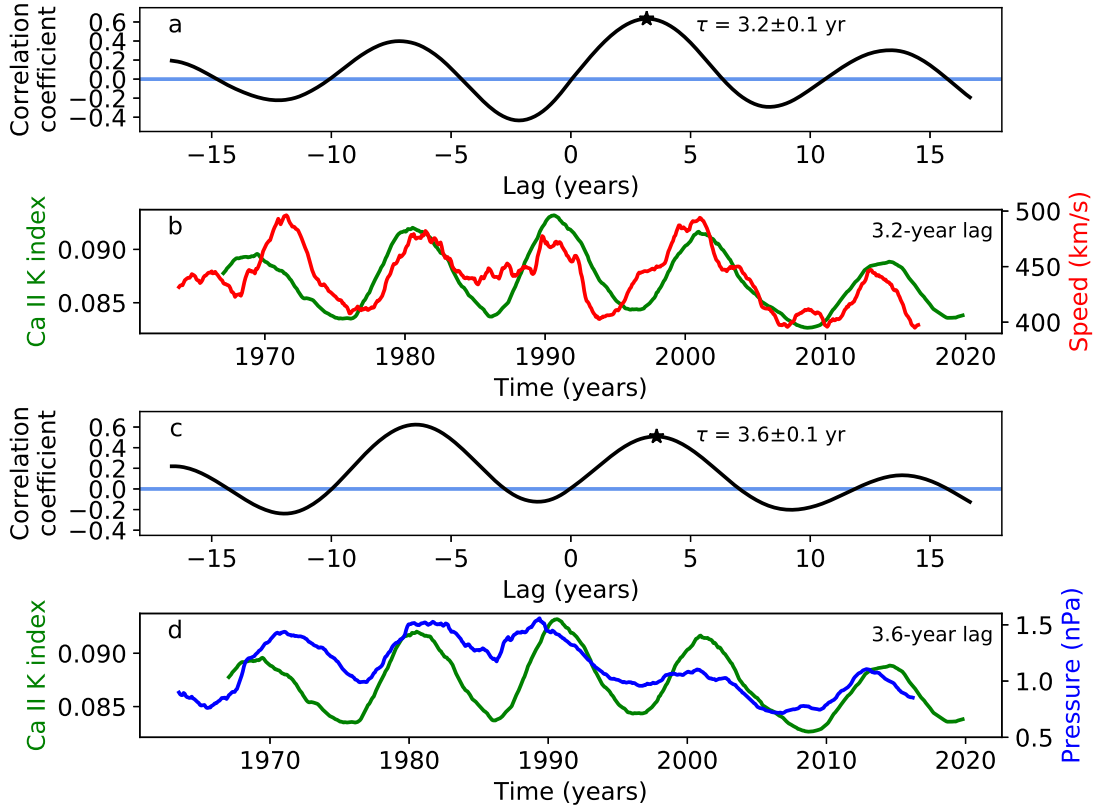


Figure 3. a) Cross-correlation between Ca II K index and Solar Wind speed. b) Solar Wind speed shifted backward with respect to Ca II K index by 3.2 years (time lag corresponding to maximum amplitude of the cross-correlation). c) Cross-correlation between Ca II K index and Solar Wind dynamic pressure. d) Solar Wind pressure shifted backward with respect to Ca II K index by 3.6 years (time lag corresponding to maximum amplitude of the cross-correlation).

of the solar wind dynamic pressure with respect to Ca II K index, as found with the cross correlation analysis, and average values for each solar cycles. The confidence intervals have been estimated taking into account the errors of the fit parameters in Eq. 3 and 4. The magnetopause standoff distance, computed by using the eq. 12 in Shue et al. (1997) and assuming the mean B_z and P values from the OMNI dataset, is shown for comparison in both panels.

The presence of the time delay makes possible to compute the stand-off distance of the magnetopause up to 2023, as shown in the upper panel of Figure 6, allowing to forecast future trend. In this sense, the estimate made with our relation shows that the average extension related to solar cycle 24 should peak in mid-2022.

The relation provided by Eq. 6 allows to use a chromospheric proxy of the solar activity to estimate the Earth's magnetospheric size and,

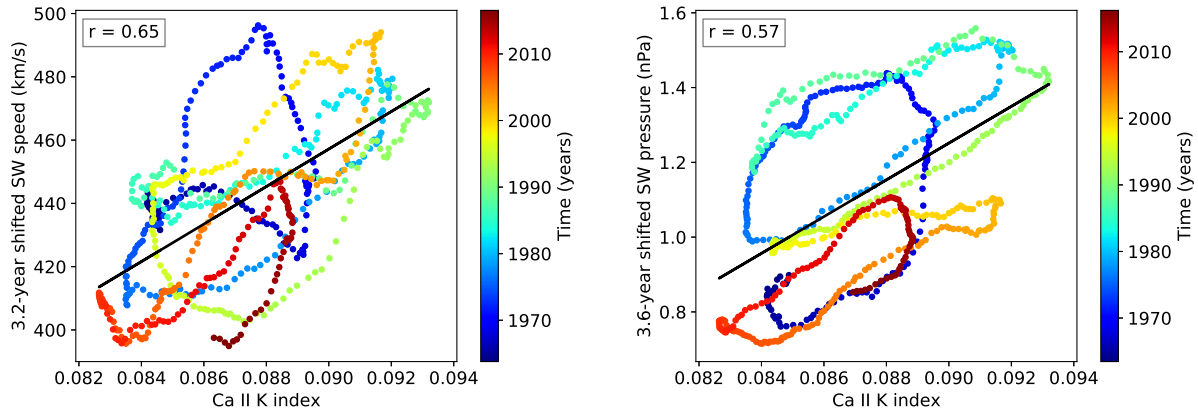


Figure 4. Scatter plot showing the relation of Ca II K index with solar wind speed (left panel) and the solar wind dynamic pressure (right panel) once the lags from cross correlation have been taken into account. The correlation coefficient is, respectively, 0.65 and 0.57. The color map shows the evolution of the relation over the time.

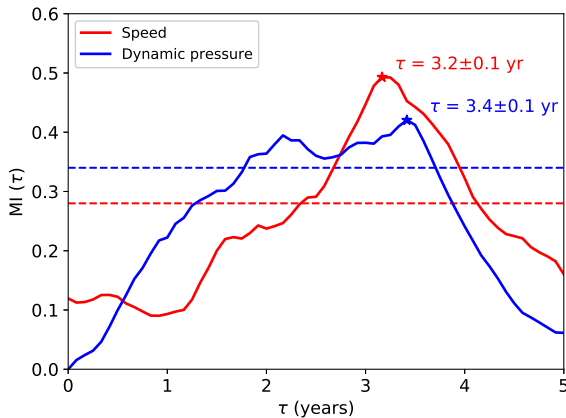


Figure 5. The mutual information coefficient between the Ca II K index and the solar wind dynamic pressure (blue line) and speed (red line). The horizontal dashed lines refer to the 95% statistical significance level.

since the Ca II K index is a physical proxy in principle measurable in each star, it can be also extended to stars with properties similar to the solar ones (i.e. Sun-like stars). Hence, this relation is very useful and it can be employed to study the effect of stellar winds on the magnetosphere of Earth-like planets orbiting stars for which similar measurements are available. To this scope a wide dataset has been provided by the HK Project at the Mount Wilson Observatory, where the emissions in the Ca II H & K lines have been monitored for a broad sample of stars and for long time intervals (up to 30 years for some stars). To test our relation in stars other than the Sun, we selected a set of ten Sun-like stars which fulfil two conditions: observations in the Ca II H & K lines are available from Mount Wilson for at least one full UV stellar cycle; they are characterized by a Rossby number $R_0 > 1$ which indicates that the star is in a faculae-dominated activity regime, like the Sun (Reinhold et al. (2019)). The spectroscopic parameters of these stars, as obtained by Valenti & Fischer (2005) and the stellar Rossby number from Marsden et al. (2014) are listed in Table 1. In order to apply our relation, we firstly computed the mean stellar S-index value and then, by using the relation by Egeland et al. (2017), for each star we calculated the Ca II K index

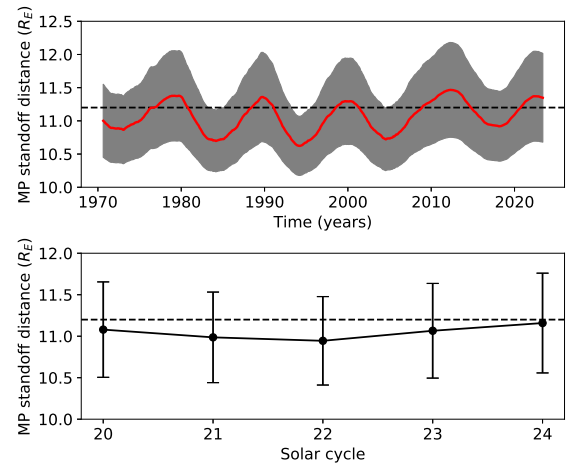


Figure 6. Earth's magnetopause standoff distance according to Eq. 6 for the time interval 1970-2023 (upper panel) and average values for the last 5 solar cycles 20-24 (lower panel). The confidence interval is shown with the shaded gray area in the upper panel and with error bars in the lower one. In both panels the dashed line shows, as reference value, the average standoff distance of the magnetopause (Shue et al. 1997).

from the S-index. Finally, by using Eq. 6 we computed the expected mean magnetopause standoff distance for hypothetical Earth-twin exoplanets orbiting at 1 AU around the host stars. As we have no direct measurements of stellar wind properties, assessing the lag between these and the UV stellar cycle is a difficult task. Therefore, using our model is not possible to determine the stellar wind properties in a specific moment in time. Nevertheless, the stars selected here have been observed for at least a full UV stellar cycle, thus the mean S-index is a robust estimate of the magnetopause standoff distance mean value. We plan to provide a more detailed analysis on a wider set of stars in an upcoming study that will include a discussion on the amplitude of the UV stellar cycle and the related stellar wind properties. The results of the present analysis can be found in the 7th column of Table 1, where we compared the magnetosphere sizes from our relation to that obtained by See et al. (2014). Starting from R'_{HK} data and by using the Parker solar wind model, they stud-

Star	Spectral type	T_{eff} (K)	log g ($cm s^{-2}$)	log R_0	Ca II K	R_{MP} (this work) (R_E)	R_{MP} (See et al. (2014)) (R_E)
HD 10780	K0 V	5327 ± 44	4.54 ± 0.06	$+0.124^{+0.000}_{-0.000}$	0.164 ± 0.017	8.63 ± 0.29	8.83
HD 100180	G0 V	5989 ± 44	4.38 ± 0.06	$+0.290^{+0.000}_{-0.000}$	0.089 ± 0.012	10.91 ± 1.03	10.74
HD 13043	G2 V	5897 ± 44	4.27 ± 0.06	$+0.324^{+0.000}_{-0.004}$	0.078 ± 0.011	12.05 ± 1.91	10.06
HD 179958	G4 V	5760 ± 44	4.39 ± 0.06	$+0.324^{+0.016}_{-0.017}$	0.080 ± 0.011	11.77 ± 1.63	11.02/10.59
HD 185144	G9 V	5246 ± 44	4.55 ± 0.06	$+0.253^{+0.006}_{-0.000}$	0.125 ± 0.014	9.38 ± 0.42	9.75/9.50
HD 34411	G1.5 V	5911 ± 44	4.37 ± 0.06	$+0.347^{+0.534}_{-0.119}$	0.076 ± 0.011	12.37 ± 2.29	10.8
HD 71148	G5 V	5818 ± 44	4.29 ± 0.06	$+0.290^{+0.009}_{-0.010}$	0.102 ± 0.012	10.16 ± 0.64	10.56/10.15
HD 76151	G3 V	5790 ± 44	4.55 ± 0.06	$+0.169^{+0.008}_{-0.000}$	0.137 ± 0.015	9.10 ± 0.37	10.07/9.30
HD 86728	G3 V	5700 ± 44	4.29 ± 0.06	$+0.340^{+0.004}_{-0.000}$	0.076 ± 0.011	12.37 ± 2.29	10.83
HD 9562	G1 V	5939 ± 44	4.13 ± 0.06	$+0.390^{+0.004}_{-0.000}$	0.071 ± 0.011	13.61 ± 4.44	10.74

Table 1. Column 1: star ID; Column 2: spectral type according to SIMBAD; Columns 3 and 4: effective temperature and surface gravity from Valenti & Fischer (2005); Column 5: logarithm of the Rossby number (R_0) from Table 1 in Marsden et al. (2014); Column 6: average Ca II K index value. The last two columns show the comparison of the magnetospheric standoff distances from this work and from See et al. (2014) for fictitious Earth-twin planets orbiting these stars. In the last column, stars with large activity ranges are listed with minimum and maximum standoff distances.

ied the effect of stellar winds on the magnetospheric extension of fictitious Earth-like planets orbiting a sample of stars, including the subset of ten stars we selected for this case study. Considering that the typical error associated to the magnetosphere sizes computed by See et al. (2014) can be estimated as $\pm 0.4 R_E$ from their Fig. 1, we can conclude that our results are in agreement within the confidence intervals.

5 DISCUSSION AND CONCLUSIONS

In the present article we introduce a convenient relationship to deduce the long-term variability of the solar wind by studying its correlation with the solar magnetic activity. To this scope the use of a physical proxy that measures the chromospheric emission in the Ca II K resonance line has been preferred to the SunSpot Number. A relationship between two solar wind parameters, speed and dynamic pressure, and the Ca II K index covering almost 5 solar cycles has been studied using 37-month averaged data.

For the overall time interval no correlation seems to exist between solar activity and both solar wind parameters, but a deeper analysis based on cross-correlation and mutual information analysis has shown that the solar wind properties follow the solar activity behaviour with a time lag of 3.2-year for the speed and 3.6-year for the dynamic pressure, respectively. Finally, taking into account the effects of the lags, we brought out a correlation relation between Ca II K index and solar wind speed (dynamic pressure) which is valid for the whole time interval.

Having a relationship that links the solar wind variations to that of Ca II K index is remarkable both for an historical reconstruction of the solar wind parameters and to even filling gaps for which measurements are not available. In particular, the solar Ca II K index is available since the beginning of the 20th century, but it has been synthetically reconstructed since 1750 in Berrilli et al. (2020) by using different solar atmospheric models that represent quiet and magnetic regions. Furthermore, the time-shifted relations obtained can be employed for an attempt at short-time predictions into the future (up to 1.7 years for speed and 2.1 years for dynamic pressure). Those predictions could be very useful to assess the mean solar wind conditions from the point of view of human space missions, but also to forecast solar wind parameters during the flight phase of Sun focused mission like Parker Solar Probe or Solar Orbiter, as in Venzmer & Bothmer (2018). In particular our model predicts a min-

imum in the solar wind dynamic pressure in mid-2022.

We believe that these results are not only helpful to achieve a better knowledge of the interaction between Sun and Earth, but also to develop new skills to study the space-climate variability of other solar-type stars, in particular those with exoplanets, enabling us to characterize the interactions between planets and their host stars and the wind conditions of exoplanetary environment. In analogy to the case of the Sun, by making use of the relations we found, the variation and hence the effects of the stellar wind of Sun-like stars on their planets can be studied by analyzing the temporal evolution of the chromospheric measurements already collected for several targets. Given the impossibility to obtain in-situ measurements of the stellar wind, it is difficult to recover the phase lag between stellar UV emission and stellar wind properties, and thus the stellar wind level in a precise moment in time. Nevertheless, having the information on at least a complete UV stellar cycle, our model enables to compute the mean magnetospheric standoff distance for planets nearby Sun-like stars.

In addition, it is useful to point out that asteroseismic observations, like those obtained by the successful photometric space missions, i.e., *Kepler* (Borucki et al. 2010) or TESS (Ricker et al. 2014), could also be used in combination with the present method to study the variation of the magnetic activity of Sun-like stars. In fact, it has been demonstrated by Bonanno et al. (2014) for a sample of 19 Sun-like stars, the presence of clear relations between the S-index and some asteroseismic parameters such as the amplitude of the observed acoustic oscillation modes or the 'small frequency separation', known as age indicator. The targets selected in Table 1 have been observed by TESS in 120 s and 20 s cadence mode and the asteroseismic analysis will be considered in the next future for a comparison with the present results. Clearly, this will open an independent way to estimate the erosion of exoplanetary atmospheres. Thus, we plan for the future to extend the present analysis to a wider set of stars, by exploiting the relationship between solar wind properties and UV emission over the Mount Wilson Observatory (MWO) measurements, which regularly observed the Ca II H & K emission since 1966 (Wilson 1978) for several stars of different spectral types. Further, in order to complete the phenomenological scenario we will complement and verify our results by employing the independent procedure based on the asteroseismic method.

ACKNOWLEDGEMENTS

RR and PG are PhD students of the PhD course in Astronomy, Astrophysics and Space Science, a joint research program between the University of Rome “Tor Vergata”, the Sapienza University of Rome and the National Institute of Astrophysics (INAF).

DATA AVAILABILITY

The Time series of the Ca II K index uses SOLIS data obtained by the NSO Integrated Synoptic Program (NISP), downloaded from the SOLIS website (<https://solis.nso.edu/0/iss/>; Monthly-Averaged ISS/SP/KKL Ca II K 1Å Emission Index Time Series). NISP is managed by the National Solar Observatory, which is operated by the Association of Universities for Research in Astronomy (AURA), Inc. under a cooperative agreement with the National Science Foundation. The Mg II composite is available from the University of Bremen (<http://www.iup.uni-bremen.de/UVSAT/Datasets/mgii>). The OMNI data are available from Coordinated Data AnalysisWeb (CDAWeb; <http://cdaweb.gsfc.nasa.gov>). The datasets of the HK Project at the Mount Wilson Observatory are available from the National Solar Observatory (NSO) website (<https://nso.edu/data/historical-data/mount-wilson-observatory-hk-project/>).

REFERENCES

- Airapetian V. S., et al., 2020, *International Journal of Astrobiology*, **19**, 136
- Baliunas S. L., et al., 1995, *ApJ*, **438**, 269
- Bavassano B., Pietropaolo E., Bruno R., 1998, *J. Geophys. Res.*, **103**, 6521
- Berrilli F., Criscuolo S., Penza V., Lovric M., 2020, *Sol. Phys.*, **295**, 38
- Bertello L., Pevtsov A., Tlatov A., Singh J., 2016, *Sol. Phys.*, **291**, 2967
- Bigazzi A., Cauli C., Berrilli F., 2020, *Annales Geophysicae*, **38**, 789
- Blanc M., Kallenbach R., Erkaev N. V., 2005, *Space Sci. Rev.*, **116**, 227
- Bonanno A., Corsaro E., Karoff C., 2014, *A&A*, **571**, A35
- Borucki W. J., et al., 2010, *Science*, **327**, 977
- Bothmer V., Daglis I. A., 2007, *Space Weather – Physics and Effects*, doi:10.1007/978-3-540-34578-7.
- Bruno R., Carbone V., 2016, *Turbulence in the Solar Wind. Lecture Notes in Physics* Vol. 928, doi:10.1007/978-3-319-43440-7.
- Bryans P., McIntosh S. W., Brooks D. H., De Pontieu B., 2020, *ApJ*, **905**, L33
- Burch J. L., Moore T. E., Torbert R. B., Giles B. L., 2016, *Space Sci. Rev.*, **199**, 5
- Dmitriev A. V., Veselovsky I. S., Suvorova A. V., 2005, *Advances in Space Research*, **36**, 2339
- Dudok de Wit T., Kretzschmar M., Liliensten J., Woods T., 2009, *Geophys. Res. Lett.*, **36**, L10107
- Duncan D. K., et al., 1991, *ApJS*, **76**, 383
- Durney B. R., Mihalas D., Robinson R. D., 1981, *PASP*, **93**, 537
- Echer E., Gonzalez W. D., Gonzalez A. L. C., Prestes A., Vieira L. E. A., dal Lago A., Guarnieri F. L., Schuch N. J., 2004, *Journal of Atmospheric and Solar-Terrestrial Physics*, **66**, 1019
- Egeland R., Soon W., Baliunas S., Hall J. C., Pevtsov A. A., Bertello L., 2017, *ApJ*, **835**, 25
- El-Borie M. A., 2002, *Sol. Phys.*, **208**, 345
- Escoubet C. P., Schmidt R., Goldstein M. L., 1997, *Space Sci. Rev.*, **79**, 11
- Feynman J., 1982, *J. Geophys. Res.*, **87**, 6153
- Galuzzo D., Cagnazzo C., Berrilli F., Fierli F., Giovannelli L., 2021, *ApJ*, **909**, 191
- Gosling J. T., Asbridge J. R., Bame S. J., Feldman W. C., 1976, *J. Geophys. Res.*, **81**, 5061
- Grießmeier J. M., et al., 2004, *A&A*, **425**, 753
- Hall J. C., 2008, *Living Reviews in Solar Physics*, **5**, 2
- Hall J. C., Lockwood G. W., 1998, *ApJ*, **493**, 494
- Hirshberg J., 1973, *Ap&SS*, **20**, 473
- Intriligator D. S., 1974, *ApJ*, **188**, L23
- Katsavrias C., Preka-Papadema P., Moussas X., 2012, *Sol. Phys.*, **280**, 623
- King J. H., 1979, *J. Geophys. Res.*, **84**, 5938
- King J. H., Papitashvili N. E., 2005, *Journal of Geophysical Research (Space Physics)*, **110**, A02104
- Köhnlein W., 1996, *Ap&SS*, **245**, 81
- Li K. J., Zhannng J., Feng W., 2016, *AJ*, **151**, 128
- Li K. J., Zhang J., Feng W., 2017, *MNRAS*, **472**, 289
- Lockwood M., Rouillard A. P., Finch I. D., 2009, *ApJ*, **700**, 937
- Luhmann J. G., et al., 2009, *Sol. Phys.*, **256**, 285
- Marsden S. C., et al., 2014, *MNRAS*, **444**, 3517
- Neugebauer M., 1981, *Fundamentals Cosmic Phys.*, **7**, 131
- Oláh K., Kóvári Z., Petrovay K., Soon W., Baliunas S., Kolláth Z., Vida K., 2016, *A&A*, **590**, A133
- Parks G. K., 2018, *Characterizing Space Plasmas*, doi:10.1007/978-3-319-90041-4.
- Petrinec S. P., Song P., Russell C. T., 1991, *J. Geophys. Res.*, **96**, 7893
- Poletto G., 2013, *Journal of Advanced Research*, **4**, 215
- Radick R. R., Lockwood G. W., Skiff B. A., Baliunas S. L., 1998, *ApJS*, **118**, 239
- Reinhold T., Bell K. J., Kuszlewicz J., Hekker S., Shapiro A. I., 2019, *A&A*, **621**, A21
- Richardson I. G., Cane H. V., 2012, *Journal of Space Weather and Space Climate*, **2**, A01
- Richardson J. D., Paularena K. I., 2001, *Journal of Geophysical Research (Space Physics)*, **106**, 239
- Ricker G. R., et al., 2014, in Oschmann Jacobus M. J., Clampin M., Fazio G. G., MacEwen H. A., eds, *Society of Photo-Optical Instrumentation Engineers (SPIE) Conference Series* Vol. 9143, *Space Telescopes and Instrumentation 2014: Optical, Infrared, and Millimeter Wave*. p. 914320 ([arXiv:1406.0151](https://arxiv.org/abs/1406.0151)), doi:10.1117/12.2063489
- Russell C. T., 1993, *Reports on Progress in Physics*, **56**, 687
- Saar S. H., Brandenburg A., 1999, *ApJ*, **524**, 295
- Samsonov A. A., Bogdanova Y. V., Branduardi-Raymont G., Safrankova J., Nemecek Z., Park J. S., 2019, *Journal of Geophysical Research (Space Physics)*, **124**, 4049
- See V., Jardine M., Vidotto A. A., Petit P., Marsden S. C., Jeffers S. V., do Nascimento J. D., 2014, *A&A*, **570**, A99
- Shannon C. E., 1948, *The Bell System Technical Journal*, **27**, 379
- Shue J. H., Chao J. K., Fu H. C., Russell C. T., Song P., Khurana K. K., Singer H. J., 1997, *J. Geophys. Res.*, **102**, 9497
- Siscoe G. L., Crooker N. U., Christopher L., 1978, *Sol. Phys.*, **56**, 449
- Skumanich A., 1972, *ApJ*, **171**, 565
- Stone E. C., Frandsen A. M., Mewaldt R. A., Christian E. R., Margolies D., Ormes J. F., Snow F., 1998, *Space Sci. Rev.*, **86**, 1
- Tokumaru M., Kojima M., Fujiki K., 2010, *Journal of Geophysical Research (Space Physics)*, **115**, A04102
- Tu C. Y., Marsch E., 1995, *Space Sci. Rev.*, **73**, 1
- Valenti J. A., Fischer D. A., 2005, *ApJS*, **159**, 141
- Vaughan A. H., Preston G. W., 1980, *PASP*, **92**, 385
- Vaughan A. H., Preston G. W., Wilson O. C., 1978, *PASP*, **90**, 267
- Venzmer M. S., Bothmer V., 2018, *A&A*, **611**, A36
- Verscharen D., Klein K. G., Maruca B. A., 2019, *Living Reviews in Solar Physics*, **16**, 5
- Viereck R., Puga L., McMullin D., Judge D., Weber M., Tobiska W. K., 2001, *Geophys. Res. Lett.*, **28**, 1343
- Viereck R. A., et al., 2004, *Space Weather*, **2**, S10005
- Weimer D. R., King J. H., 2008, *Journal of Geophysical Research (Space Physics)*, **113**, A01105
- Weimer D. R., Ober D. M., Maynard N. C., Burke W. J., Collier M. R., McComas D. J., Ness N. F., Smith C. W., 2002, *Journal of Geophysical Research (Space Physics)*, **107**, 1210
- Weimer D. R., Ober D. M., Maynard N. C., Collier M. R., McComas D. J., Ness N. F., Smith C. W., Watermann J., 2003, *Journal of Geophysical Research (Space Physics)*, **108**, 1026
- Wilson O. C., 1968, *ApJ*, **153**, 221
- Wilson O. C., 1978, *ApJ*, **226**, 379

This paper has been typeset from a \TeX/L\AA\TeX file prepared by the author.

This figure "MI.png" is available in "png" format from:

<http://arxiv.org/ps/2203.01554v1>

This figure "MP_standoff_distance.png" is available in "png" format from:

<http://arxiv.org/ps/2203.01554v1>

This figure "cross_correlation.png" is available in "png" format from:

<http://arxiv.org/ps/2203.01554v1>

This figure "scatter_color_map_ca-p.png" is available in "png" format from:

<http://arxiv.org/ps/2203.01554v1>

This figure "scatter_color_map_ca-v.png" is available in "png" format from:

<http://arxiv.org/ps/2203.01554v1>

This figure "shifted_scatter_plot_ca-p.png" is available in "png" format from:

<http://arxiv.org/ps/2203.01554v1>

This figure "shifted_scatter_plot_ca-v.png" is available in "png" format from:

<http://arxiv.org/ps/2203.01554v1>

This figure "signals.png" is available in "png" format from:

<http://arxiv.org/ps/2203.01554v1>